THE JOURNAL OF PHYSICAL CHEMISTRY C

Article

pubs.acs.org/JPCC

Is Antidot-Patterned Graphene Aromatic? Unusual Aromatic Properties of Graphene Antidot Lattices and Antidot-Functionalized Nanographenes

Aristides D. Zdetsis*[,†,‡] and E. N. Economou[‡]

[†]Molecular Engineering Laboratory, Department of Physics, University of Patras, Patras 26500 GR, Greece

[‡]Institute of Electronic Structure and Laser, Foundation for Research & Technology Hellas, Vassilika Vouton, P.O. Box 1385, Heraklion, Crete GR-71110, Greece

ABSTRACT: On the basis of our recent predictions for a coupled resonance aromaticity pattern of graphene (*J. Phys. Chem. C* **2015**, *119*, 16991), we have studied the anticipated breaking or uncoupling of such dual patterns induced by the presence of particular antidots arranged periodically in a graphene or nanographene film, using numerous properly selected microscopic real-space models in the framework of ab initio density functional theory (DFT). We found that the aromaticity pattern of the antidots is literally tuned to the Clar-type primary aromaticity pattern of graphene, generated by repeated motifs of the hexagonal circumcoronene (CIRCO) pattern, in such a way that the centers of the CIRCO motifs coincide with the centers of the antidots. Thus, the aromaticity pattern of the antidot lattice consists of the isolated primary CIRCO pattern of graphene. However, the nature of the aromaticity and the related bonding and banding characteristics are largely dependent on the degree of antidot passivation, a subject that is grossly overlooked in the literature. For totally nonpassivated antidots, in contrast to the fully passivated ones, we show that the resulting CIRCO aromaticity pattern is dominated by σ aromaticity rooted in the dangling bonds of the antidots, which is of the Clar type, even though Clar's rules were devised for common π aromaticity. On the other hand, the π aromaticity of the fully passivated antidots, the ones commonly studied in the literature, is very much determined by the aromaticity pattern of the "parent" structure. Thus, the overall aromatic and electronic characteristics of fully passivated finite antidot-decorated nanographenes, similarly to those of the intact nanographenes, are practically determined from the aromaticity pattern of the intact parent nanographene, which, as we illustrated earlier, shows a three-member periodicity in which most of the known periodicities in the properties of nanographenes, nanoribbons, and nanotubes are rooted. It is concluded, therefore, that most or all of the rules for gap opening based on aromaticity and/or chirality in reality stem from these aromatic periodicities.

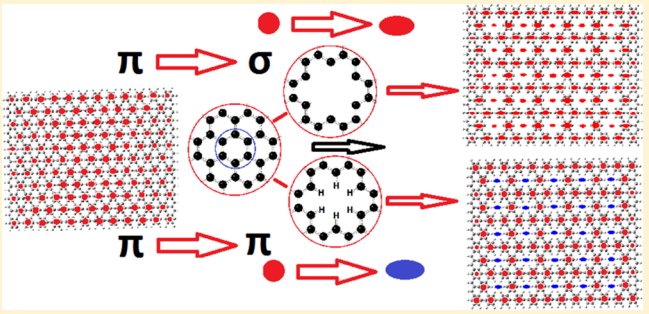

1. INTRODUCTION

The subject of the aromaticity of graphene[1,2] (and graphite[3]) and graphene-based structures is intriguing but elusive, primarily because aromaticity itself is a controversial molecular (not crystalline) property that is not directly measurable.[4,5] Furthermore, graphene itself is a peculiar crystal/molecule with "exotic" electronic properties[6,7] that, according to the early suggestion of Pauling,[8] should have been characterized as a resonance structure but that, according to Moran et al.,[3] should be considered superaromatic because the resonance energy per π electron of graphite is greater than that in benzene.[3] Recently, Popov et al.[2] considered the question of the aromaticity of graphene by examining small, highly electron-depleted nanographene fragments such as $C_6H_6^{4+}$, $C_{24}H_{12}^{10+}$, and $C_{54}H_{18}^{16+}$ that have two electrons per ring and concluded that graphene is indeed aromatic, but only locally, with two π electrons localized over each ring. More recently, we[1] also examined the question of the aromaticity of graphene through a process of "spatial evolution" of suitably selected graphene models of successively increased size, using a simple but well-established method based on nucleus-independent chemical shifts (NICS).[4,5] We found that graphene is indeed aromatic and is certainly a type of resonance structure, in agreement with the expectations of Pauling, resonating between a primary aromaticity pattern consisting of multiple circumcoronene (CIRCO) aromaticity patterns, fully consistent with Clar's aromatic sextet theory, and a complementary coronene (CO) type of pattern compatible with "migrating sextets". Clearly, such behavior is well beyond the concepts of local and global aromaticity but in agreement with the findings of Zubarev et al.,[9] who concluded that aromaticity in graphene is primarily a collective effect that can give rise to self-organized criticality (SOC).

We further illustrated[1] that, for finite (nanographene) or semi-infinite (e.g., nanoribbon and nanotube) graphene-based

Received: November 5, 2015
Revised: December 15, 2015
Published: December 16, 2015

DOI: 10.1021/acs.jpcc.5b10842
J. Phys. Chem. C 2016, 120, 756−764

structures where the periodicity is interrupted (e.g., at the boundaries) or modified, the coupling of the CIRCO and CO patterns is no longer operative and the CIRCO primary pattern is fully revealed at the proper size and symmetry.[1] As a result, it was shown[1] that periodic variations occur in the aromaticity patterns in terms of the size or periphery of finite-size nanographenes, which is responsible for the analogous periodicities found in graphene nanoribons[10,11] and nanotubes,[12] all stemming from the same primary aromaticity pattern.[1] Thus, the electronic and aromatic properties, and in particular the band gaps, of graphene and graphene-based structures can be properly tuned (functionalized) by suitably adjusting their size and periphery. Aside from size adjustment, another method of uncoupling and literally "tuning" (as shown below) the aromaticity pattern of graphene is by periodic patterning using in particular nanoscale perforation. This approach is considered particularly promising[13−18] for band-gap engineering. Pedersen and co-workers[13,14,18] concluded that a periodic array of holes (antidot lattice) renders graphene semiconducting with a controllable band gap. Such antidot lattices are a well-studied class of man-made structures (metamaterials) with very interesting properties.[18−22] Graphene sheets with regularly spaced holes ("antidots") would be expected to display similar phenomenology, but within a much more favorable energy scale.[14] As illustrated below, in agreement with later reports,[16] the gap is not always increasing in the antidot lattice. Yet, as we found in the present investigation, several new unforeseen factors, such as the interplay between σ and π aromaticity and the degree of hole passivation, practically determine the electronic and aromatic properties of the antidot lattices. We illustrate here that, aside from the rich technological significance of antidot lattices, the subject is of purely scientific importance, stemming from the uncoupling of the CIRCO and CO patterns (see Figure 1 below), as was predicted in our earlier work.[1] In the present investigation, we use the same method and techniques, and, as before,[1] to avoid unnecessary debates as to the proper method for evaluating aromaticity and so on, we stick to the choice of the NICS magnetic criterion of aromaticity, believed to be the simplest, most well-established and widespread[23−25] index based on the chemical shift of aromatic ring currents induced by an magnetic field applied perpendicular to the plane of the ring(s). As a result of this choice, strictly speaking, the aromaticity/antiaromaticity described herein corresponds to magnetic aromaticity/antiaromaticity (magnetotropicity). Clearly NICS, without being free of criticism, is very accessible and easy to compute: It can be used to discuss both the local and global aromaticities of molecules; it does not use reference values; and finally, it can easily be used for both π and σ types of aromaticity.[23−26] This last characteristic is of particular importance in the present work, where we found that the aromaticity is primarily of σ type, for not fully passivated antidots (holes), which have been grossly overlooked in the literature. For such nonpassivated antidots, the tuning is almost literally so, because the centers of the antidots tend to coincide with the centers of the CIRCO units of the σ-aromaticity pattern(s), apparently to maximize the number of aromatic rings (on the rims and elsewhere). Such an aromaticity pattern (although of σ type) is fully consistent with Clar's rules, which, however, have been invoked for the common π-type aromaticity. Moreover, for the typical well-studied fully passivated antidots (in infinite- and finite-size nanographenes), we found that the aromaticity pattern is primarily tuned to the aromaticity pattern of the "parent" intact structure, which, as we have shown, belongs to a three-member periodic sequence, for rectangular $n \times n$ nanographenes with n zigzag and n armchair rings in their periphery (see Figure 10 in ref 1). In such a periodic sequence, the fully aromatic Clar-type structures correspond to ring numbers $n = 1$ (benzene), 4, 7, 10, and so on; that is, $n = 3m + 1$, $m = 0, 1, 2, 3, \ldots$. One can therefore conclude that the various criteria in the literature[15−17] for band-gap opening based on aromaticity and/or chirality[17] should, in reality, be related to and rooted in the fundamental periodicity of the aromaticity patterns of the parent structures and the tendency to have the centers of the CIRCO units coincide with the centers of the antidots. This should be very important for the ideal design of antidots.

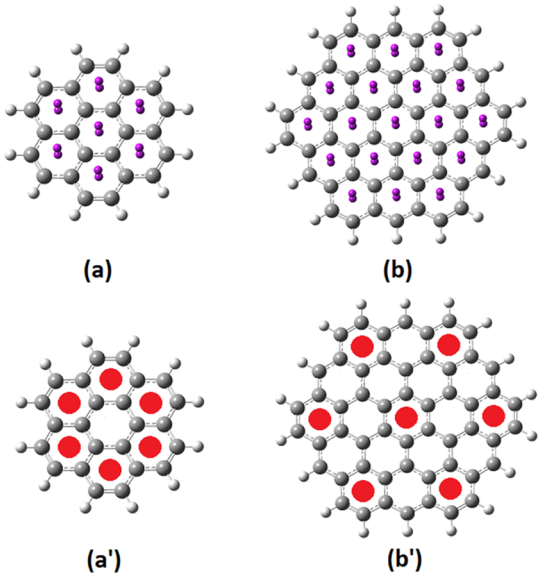

Figure 1. (a,b) Network of "dummy atoms", represented by small purple spheres at (and above) the centers of the hexagonal rings, used in the evaluation of NICS(0) and NICS(1) for (a) coronene (CO) and (b) circumcoronene (CIRCO). (a′,b′) Corresponding (a′) CO and (b′) CIRCO aromaticity patterns.

The current article is organized as follows: After the introduction in section 1 and the brief discussion of the methodology in section 2, the results are presented and discussed in section 3, arranged in three subsections: section 3.1 including results mainly for nonpassivated antidots, section 3.2 containing results for fully passivated antidots, and section 3.3 containing results for partially passivated antidots. Finally, the conclusions of the present work are summarized in section 4.

2. METHODOLOGY

The methodology and technical framework of the calculations were described previously.[1] The real-space models consist of most of the nanographene samples we considered in our previous investigation,[1] in which we selectively create a number of holes (antidots) that are one ring wide and have six zigzag sites on their rims, known as Z_6 antidots. We considered both hydrogen-passivated and nonpassivated antidots. As before, all density functional theory (DFT) calculations (geometries, energies, NICS) were implemented using the Gaussian program package,[27] employing the hybrid PBE0[28] functional and the 6-31G(d) basis set as used in this package. To obtain

DOI: 10.1021/acs.jpcc.5b10842
J. Phys. Chem. C 2016, 120, 756−764

the NICS values through the computation of the chemical shifts at the center of the ring(s) due to a magnetic field applied perpendicular to the plane of the ring(s), a dummy atom is usually placed at the center(s) of the ring(s), NICS(0), and 1 Å above the center of the ring(s), NICS(1), as shown in Figure 1, and the induced chemical shifts are calculated in a manner similar to that used for the usual atomic nuclear magnetic resonance (NMR) chemical shifts in NMR spectroscopy.

3. RESULTS AND DISCUSSION

3.1. Nonpassivated Antidots. In Figure 2, we show the aromaticity pattern of 6A × 8Z nanographene (see ref 1),

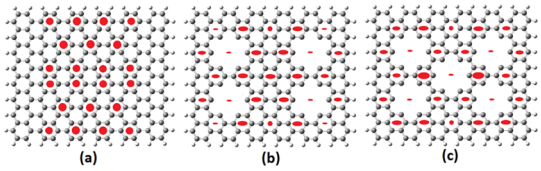

Figure 2. Aromaticity patterns of 6A × 8Z nanographene (a) without any holes, (b) with four nonpassivated holes, and (c) with five holes (without H passivation). Rings that are σ-aromatic are indicated by full ellipses (versus full circles for π-aromatic rings) with sizes proportional to the NICS magnitude.

together with the aromaticity patterns of the corresponding four and five antidots. As one can see in Figure 2b, the four-hole pattern, independently of, and in contrast to, the initial form (without the holes), tunes to and brings up the CIRCO pattern both at the center of the structure and around each of the holes, in agreement with our predictions.[1] However, the vast majority of the rings are σ-aromatic (or at least σ-dominated), with NICS(1) less negative than NICS(0).

This is corroborated by the nature of the corresponding frontier molecular orbitals (FMOs), shown in Figure 3. In the

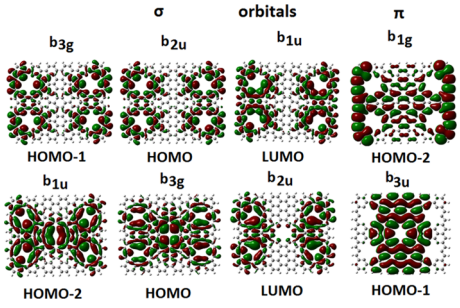

Figure 3. Three-dimensional plots of the frontier molecular orbitals of 6A × 8Z (top) four-hole and (bottom) five-hole nanographenes (isovalue = 0.01).

particular cases of four and five holes in 6A × 8Z nanographene, both the HOMO and LUMO are σ molecular orbitals (σ MOs), whereas the HOMO − 2 for four holes and the HOMO − 1 orbital for five holes are π molecular orbitals (π MOs), as can be verified by their respective symmetries in the D_{2h}-symmetric nanographene structures (b_{1u}, b_{2u}, and b_{3g} are symmetric with respect to reflections through the xy plane, in contrast to b_{1g} and b_{3u}, which are antisymmetric). In other cases, either the HOMO or the LUMO or both are π orbitals. Thus, the overall energy gap here, in contrast to the "pure π gap" of the various intact nanographenes, depends on the relative magnitude of the σ and π gaps and widths, which are clearly determined by the antidot arrangement in the parent structure. This is not the case for the fully passivated antidot arrays, as will be shown later in section 3.2. In Figure 3, one can also see that the σ MOs are delocalized over the holes, whereas the π orbitals are localized in the region between holes, as would be expected.

Furthermore, from Figure 2, one can see that the central portion is more aromatic than the left and right sides near the zigzag edges, as reflected in the sizes of the ellipses. The centers of the holes, as one can verify from Table 1, are clearly very

Table 1. Representative (Large, Small, Central) NICS(1) and NICS(0) Values and HOMO−LUMO Gaps (H−L)[a,b]

	NICS(1)/NICS(0) (ppm)			
structure	large	small	central	H−L (eV)
(1) 6 × 8 $C_{204}H_{40}$	−14.6	−11.2		0.32
	−12.1	−8.2		
(1a) 6 × 8 four holes	−13.0	−3.6	−14.6	0.17
	−20.9	−5.6	−16.1	
(1b) 6 × 8 five holes	−24.2	−5.7	−4.3	0.15
	−53.0	−7.8	−8.6	
(2) 10 × 10 $C_{420}H_{60}$	−15.4	−9.5	−15.3	0.15
	−12.8	−6.3	−12.3	
(2a) 10 × 10 nine orthogonal holes	−14.6	−7.8	−5.8	0.02
	−36.4	−9.1	−9.1	
(2b) 10 × 10 nine oblique holes	−16.2	−10.2	+28.4	0.08
	−31.8	−7.5	+36.2	
(3) 12 × 16 $C_{792}H_{80}$	−16.1	−11.2	−13.3	0.17
	−13.5	−9.1	−9.5	
(3a) 12 × 16 25 holes	−47.9	−7.5	−18.68	0.09
	−95.4	−11.1	−23.44	

[a]Structures 1, 2, and 3 indicate full dots. [b]For antidots, "small" values correspond to centers of noncentral holes.

weakly aromatic [i.e., very small values of NICS(1) and NICS(0)] or even nonaromatic (if very small NICS values are ignored), and in certain rare cases (see Figure 4c), they could even be antiaromatic. The same is true for the five-hole case. In both cases, the centers of the CIRCO patterns appear in the aromaticity patterns and are pinned around the holes' centers, with their peripheries on the rims. This type of selectivity in the aromaticity pattern maximizes the number of the σ-aromatic rings. In other words, the σ aromaticity is rooted in the holes' rims at and around the dangling bonds. A few (two in Figure 2b,c) π-aromatic rings appear away from the holes in the central region close to the armchair edges. This can be also seen (more clearly) in Figure 4, which shows a larger (10A × 10Z) sample (Figure 4a), together with nine antidots (Figure 4b,c). It should first emphasized that this 10 × 10 nanographene was predicted in our earlier work[1] to be fully Clar-type aromatic with a complete CIRCO aromaticity pattern, which is indeed the case, as shown in Figure 4a. Similarly to the other Clar-type (CIRCO) aromatic, the number of peripheral rings (n = 10) fits the description $n = 3m + 1$, with m = 3. In Figure 4b, one can clearly see that, away from the holes, the π aromaticity "survives" in full harmony and continuity with the σ aromaticity with which it is interlinked, and therefore, we have a $\sigma + \pi$ aromaticity type[25,26] that is globally localized. To examine the effect of antidot symmetry, in accord with the work of Ouyang et al.,[16] we consider in Figure 4c the same number of antidots (nine) in a different arrangement, so that the direction(s) of the antidot arrays do not coincide with principal symmetry

DOI: 10.1021/acs.jpcc.5b10842
J. Phys. Chem. C 2016, 120, 756−764

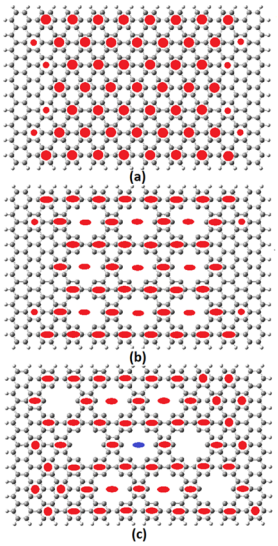

Figure 4. Aromaticity patterns of a 10A × 10Z nanographene sample (a) with no holes and functionalized with (b) six orthogonal holes and (c) six oblique holes. Full red circles indicate π aromaticity, full red eclipses denote σ aromaticity, and full blue eclipses denote σ antiaromaticity.

directions. Thus, in contrast to Figure 4a,b, where the overall symmetry is D_{2h}, in Figure 4c, the symmetry is C_{2v}. As one can see in Figure 4, all of the basic conclusions about the pinning of the aromaticity pattern around the holes and the $\sigma + \pi$ nature of the aromaticity patterns remain unchanged. The only observable change in the aromaticity pattern is the antiaromaticity of the central hole, together with the diminishing aromaticity (very small values of NICS) in the centers of the holes of the horizontal central array and at the centers of the holes closer to the zigzag edges, which is in agreement with our previous finding[1] that the regions around the zigzag edges are less aromatic. From Table 1, one can also see that the HOMO−LUMO gap of the structure in Figure 4c, although very small and smaller than that of the intact structure (Figure 4a), it is still larger than the higher- (D_{2h}) symmetry holes in Figure 4b. Thus, although the structure in Figure 4c with the lower symmetry is the only one, from all of the structures examined here, with the central antidot clearly antiaromatic and the central array nonaromatic, it still follows the same rules, and the σ orbitals (responsible for the σ aromaticity) are concentrated around the holes, as shown in Figure 5. All FMOs shown in Figure 5 for the oblique holes are of σ type. For the orthogonal holes, the HOMO − 1, HOMO, and LUMO + 1 are of π type. The larger gap of the oblique holes compared to the orthogonal ones could be related to the larger number of π-aromatic rings, as can be seen in the aromaticity

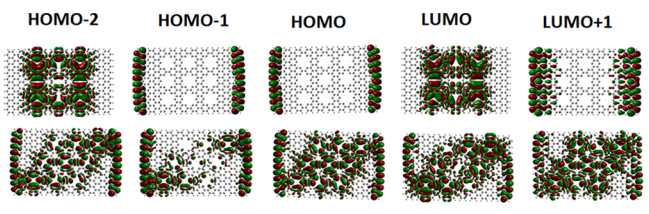

Figure 5. Three-dimensional plots of the frontier orbitals of 10 × 10 nanographene, patterned with nine holes: (top) orthogonal and (bottom) oblique.

patterns in Figure 4b,c. However, energetically the orthogonal holes are 2.2 eV lower (perhaps due to the nonaromaticity/antiaromaticity of the holes in the central region). This is not as strange as it seems at first sight, because (cohesive) stability, aromaticity, and HOMO−LUMO gaps (measuring "kinetic" stability) are known not to be always compatible.[29]

All of the characteristics described thus far are common in the vast majority of nanographenes with antidots (holes) examined here, including almost all of the nanographenes considered in our previous study[1] and many more (such as the 10 × 10 structure in Figures 4 and 5).

The general conclusions are always the same:

Each nonpassivated hole in graphene usually creates either a full CIRCO pattern of σ aromaticity, in which the central ring is relatively weakly aromatic (typical NICS values around −6 or −5 ppm) or (more commonly) a CIRCO pattern that is truncated at the center, in which the central ring is nonaromatic with NICS values close to zero whereas all "peripheral" CIRCO rings (in full accord with Clar's rules) are fully aromatic but of σ type. We can humorously call this truncated CIRCO pattern "holly" or HCIRCO. The large majority of nonfully passivated holes create complete CIRCOs or HCIRCOs around their center of σ aromaticity. In very rare cases, the development of full CIRCOs or HCIRCOs is frustrated by severe size and/or symmetry restrictions, resulting in incomplete CIRCOs or HCIRCOs, or even antiaromatic rings sometimes, which, as will be seen below, are energetically nonfavored. The rings in the region away from the holes are usually π-aromatic, forming normally full CIRCO patterns, in harmony with their σ-aromatic neighboring rings, if geometrical and size restrictions allow. In several cases, the CIRCOs or HCIRCOs are composed of both π- and σ-aromatic rings. All of these variations clearly illustrate the importance of σ bonding in the structural and geometrical (D_{6h} symmetry) characteristics of graphene (with and without holes) and even of benzene itself. In fact, the present data seem to support the conclusions of Maksić et al.[30] that the Clar sextet rule is a consequence of the sp^2 σ-electron framework. The importance of the sp^2 honeycomb framework in graphene and other two-dimensional materials is also illustrated in the BC_3 honeycomb epitaxial sheet[31] and the fluorinated C_4F graphene sheet,[32] among others. As shown by Boldyrev and collaborators[31,32] using the adaptive natural density partitioning (AdNDP) method, in these cases, there are π-empty hexagonal rings (with only σ bonding). As a result, there is a higher number of π electrons in the full hexagons, approaching the number of π electrons in benzene (six) rather than graphene (where the corresponding number is two). This process was called the "benzation" of graphene. One could perhaps imagine that the "empty" rings (or "anti-rings") of the missing hexagons of the holes could, in a sense, be remotely related through an "analogous" behavior, at least in part, with the empty hexagons in BC_3, C_4F, and other planar species. However, this is conjecture that is clearly outside the scope of the present investigation.

Apparently, all of the aromatic characteristics described above are basically independent of the size of the holly nanographene. To be able to generalize to the "complete" antidot lattice, we need to construct a large, fully covered antidot structure. This was accomplished in the present study with a full 25-hole lattice completely covering the 12A × 16Z nanographene structure, which is the largest real-space structure we have considered in our work to date.[1] As one can see in Figure 6, in a full antidot lattice, the σ aromaticity is

DOI: 10.1021/acs.jpcc.5b10842
J. Phys. Chem. C 2016, 120, 756−764

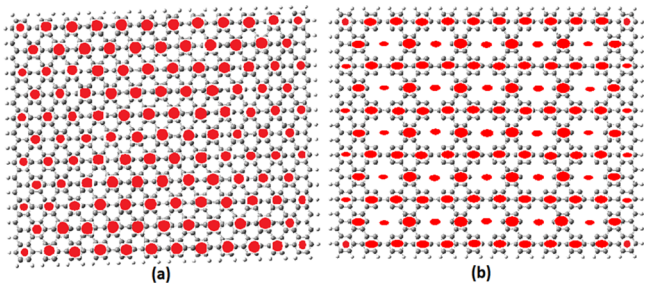

Figure 6. Aromaticity patterns of (a) full graphene and (b) antidot graphene "lattices". Following the convention used in the previous figures, σ-aromatic rings are indicated by full ellipses (versus full circles for π-aromatic rings) with sizes proportional to the NICS magnitude.

dominant, and the σ-aromaticity pattern is similar and analogous (almost identical) to the full graphene's primary π-aromatic CIRCO (Clar-type) aromaticity pattern, as was predicted in ref 1.

As can be verified from the results in Table 1, the NICS(1) values at the centers of the noncentral antidots are characterized by relatively weakly aromatic values, with an NICS(1) value of about −7.5 ppm and an NICS(0) value of about −11.1 ppm. These NICS values are of very small magnitude compared to the largest σ NICS(1) and NICS(0) values, which are about −48 and −95 ppm, respectively. This is why, in several cases where the relative differences are large, there are HCIRCOs instead of CIRCOs.

The corresponding frontier orbitals for the antidot lattice are shown in Figure 7. All of them are of σ type, as could be expected, and all of them are extended from one edge to the other. This could be very important for their transport properties.

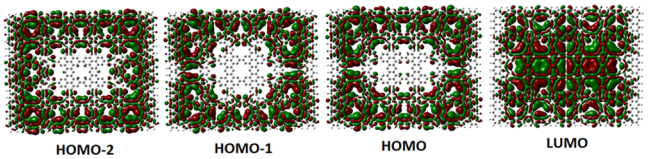

Figure 7. Three-dimensional plots of the frontier molecular orbitals (HOMO − 2, HOMO − 1, HOMO, LUMO) of the 25 holes in 12A × 16Z nanographene, representing the antidot lattice.

From the results presented so far, it becomes clear that, by selecting the location of the antidots' centers, we are actually (pre)selecting the centers of the CIRCO patterns to be developed (if geometrical conditions and size restrictions allow), and this is very important for applications. For fully aromatic "parent nanographenes" of the CIRCO (or Clar) type in which the CIRCO and hole centers coincide, as in Figures 4b and 6b, the hole centers are substantially aromatic. Otherwise, as in Figure 2b,c, the hole centers are nonaromatic or even antiaromatic. It should be emphasized that, as is shown in Table1, in the majority of the cases examined so far, the overall HOMO−LUMO gap decreases in relation to the corresponding gap for intact nanographene rather than increasing, in contrast to most of the earlier reports[13−17] but in accord with the conclusions of Ouyang et al.[16] However, with the exception of ref 17, practically all of the previous theoretical work in antidots[13−17] (including ref 16) was almost exclusively dedicated to fully passivated (with hydrogen) holes, which we have not considered here thus far. In reality, one would expect to have some sort of partial or even complete passivation. Therefore, we need to examine and compare the same models of antidots for the cases of fully (and/or partially) passivated antidots. This is done in the next two subsections.

3.2. Fully Passivated Antidots. In Figure 8, we show the analogue of Figure 2 but for fully passivated antidots. As one

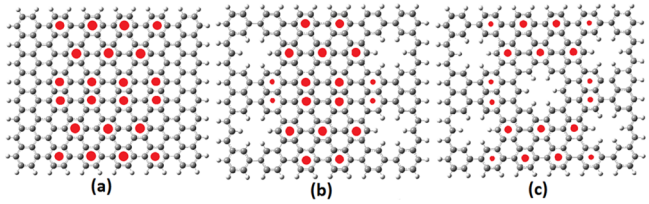

Figure 8. Aromaticity pattern of 6A × 8Z nanographene (a) without holes, (b) with four H-passivated holes, and (c) with five holes (with H-passivation).

can see in Figure 8, in this case, the primary π-type aromaticity pattern of the intact lattice remains practically frozen, and the antidots are characterized by exactly the same aromaticity pattern, except for the missing initial aromatic rings, which are now open because of the antidots. The centers of the antidots are "nonaromatic" (marginal values of NICS) or (more commonly) weakly antiaromatic (marginal positive values of NICS).

The aromaticity in this case is clearly and fully of π type. There is no σ aromaticity whatsoever, because σ aromaticity is associated with unsatisfied dangling bonds. Furthermore, it is rather striking to realize that, for fully passivated antidots, the aromaticity pattern in both cases (four and five holes) remains practically the same as that of the parent structure, save the holes. This is common to the majority of the structures examined here. It is therefore tempting to assume that the aromatic characteristics, which are usually associated with band-gap size, are practically determined more from the parent structure and much less from the details of the hole arrangement, which seems to be quite common. This is also verified by the structure of the frontier orbitals, in comparison to the corresponding parent intact nanographene orbitals, shown in Figure 9. As one can see in this figure, these orbitals (save the holes) are practically identical. Moreover, because both the HOMO and LUMO are dominated by "surface" (zigzag) edge orbitals, to further emphasize the similarity of the parent−daughter orbitals, in Figure 9, we also include the corresponding "bulk" effective HOMO−LUMO gap (skipping the surface-localized orbitals that are closest to the HOMO and

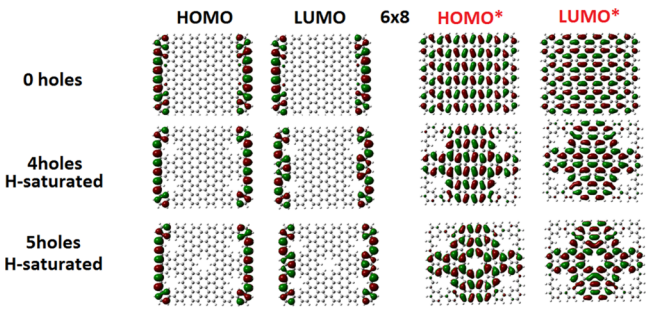

Figure 9. Three-dimensional plots of the HOMO and LUMO and bulk effective HOMO and LUMO (HOMO*, LUMO*) (see text) for zero, four, and five fully passivated 6 × 8 antidots.

DOI: 10.1021/acs.jpcc.5b10842
J. Phys. Chem. C 2016, 120, 756−764

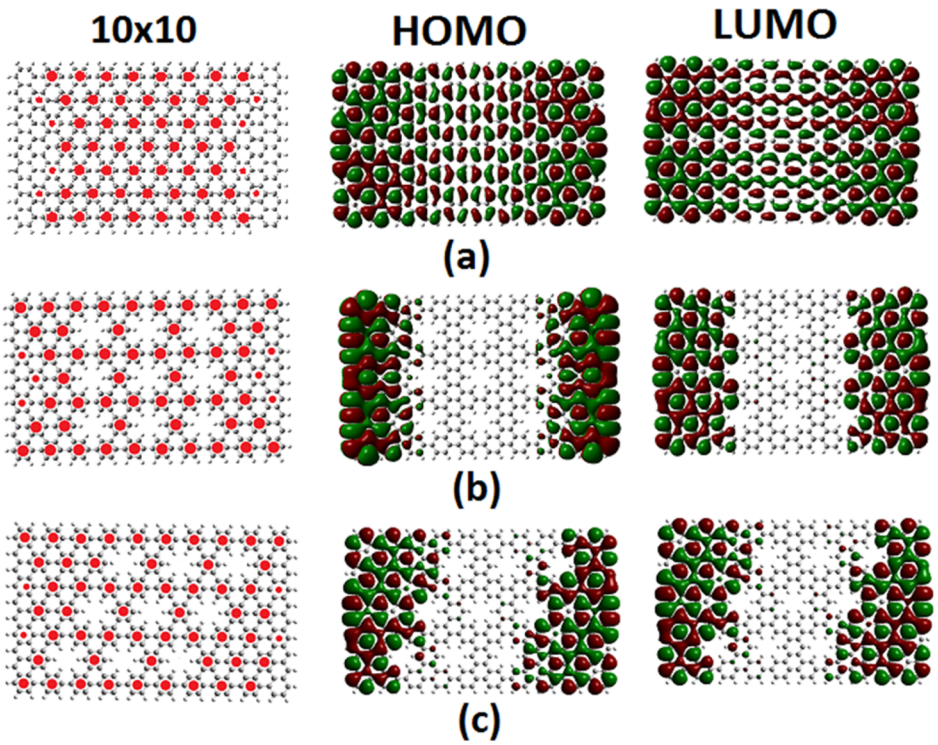

Figure 10. Aromaticity pattern and three-dimensional plots of the HOMOs and LUMOs for (a) intact 10 × 10 nanographene and (b,c) the parent structure with (b) nine orthogonal holes and (c) nine oblique holes.

LUMO "nonsurface" orbitals around the Fermi level). As one can see, the similarity is striking. Such similarity is also evident in the HOMO−LUMO gap, which is the same (0.4 eV) for both four and five holes and 0.08 eV larger than that of the parent structure. The same is true for the corresponding "effective" band gap. Obviously, the same behavior is expected for other fully passivated antidots, such as the nine antidots on the 10 × 10 nanographene that we considered earlier.

Indeed, as one can see in Figure 10, both orthogonal and oblique passivated holes have similar HOMOs, LUMOs, and HOMO−LUMO gaps (0.10 eV), and the energy difference between orthogonal and oblique holes is now only 0.22 eV (1 order of magnitude smaller than in the nonpassivated case). The centers of the holes (antidots) are relatively "weakly antiaromatic" (paratropic), that is, they have small positive NICS values of about 5−6 ppm, which we ignored in the figure, not because they are irrelevant, but for simplicity because, in absolute value, they are smaller than 70% of the corresponding NICS values of benzene (or significantly smaller in comparison to the largest absolute values of NICS). However, it should be remembered that they are indeed there and that they are very significant.

This is why, in Figure 11, which, in analogy to Figure 6, represents the aromaticity pattern of the fully passivated antidot lattice, we include all antiaromatic centers of the antidots in a separate partition (Figure 11b). Clearly, Figure 11b represents the true aromaticity pattern of the fully passivated antidot lattice, which is the most well-studied antidot structure. As one can see, the difference between Figures 6 and 11 is rather dramatic.

In view of the fact that the majority (if not the totality) of the theoretical works in the literature are devoted to fully passivated antidots, it should be desirable to compare, at least in part, our results with known results in the literature.[15−17,33−35] However,

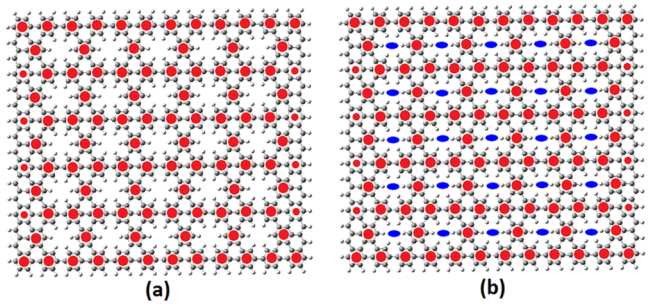

Figure 11. Aromaticity patterns of the 12A × 16Z fully H- passivated antidot lattice with 5 × 5 antidots. Solid circles indicate π-aromatic rings. In panel a, small (5−6 ppm) σ-antiaromatic (positive) NICS values (at the centers of the holes) have been ignored. In panel b, these antiaromatic NICS positions are included and indicated by solid blue ellipses.

by the very nature of the approach, such a comparison cannot be done in a direct and quantitative way, but must be done only indirectly and qualitatively. The basic reason for this is not just the limited size of our "samples", because we have illustrated that, for judicially selected properties, this can be properly taken into account and extrapolated "appropriately",[1,36] through such a process as spatial evolution.[1] It is rather obvious that the band gaps, because of edge effects and quantum confinement, cannot be safely projected onto infinite or semi-infinite samples (see, for instance, the results in Table 2 of ref 1). One could perhaps invoke the "effective bulk gaps", through the effective bulk FMOs on the right-hand side of Figure 9. However, this is not always practical or even possible for larger samples. Alternatively, one can indirectly compare the band gaps on the premise that Clar aromaticity (CIRCO pattern) is related to higher gaps, as has been illustrated in the existing literature for "similar" semi-infinite[10−12] and infinite[15−17,33−35] samples. We

DOI: 10.1021/acs.jpcc.5b10842
J. Phys. Chem. C 2016, 120, 756−764

employed this alternative method here in view of the (main) inherent difficulty of direct comparison, which is associated with the nanographene approach of our description, in which the main comparisons are between the parent nanographene structure and the particular antidots patterned on that structure. This is completely new, because practically all existing literature reports of which we are aware deal with the infinite (passivated) antidot lattice, in comparison to infinite graphene. There is no such analogue of the parent structure in the existing literature calculations and, therefore, no full direct comparison. Yet, all fundamental conclusions and basic (seemingly diverse) criteria that can be checked indirectly are in accord with our conclusions, basically because they all stem from the fundamental primary Clar-type CIRCO aromaticity pattern.

We have shown that, for tetragonal $N \times N$ or rectangular $M \times N$ graphene dots (nanographenes), the CIRCO (Clar) pattern occurs in a three-member periodic cycle, every time N is of the form $N = 3n + 1$ ($n = 0, 1, 2, 3, ...$). For fully passivated (Z_6) antidots, the "maximum-aromaticity" condition is obtained when the centers of the antidots coincide with aromatic rings of the parent structure and, in particular, when the condition $N = 3n + 1$ is fulfilled. It is clear, however, that, for a given (arbitrary) arrangement of antidots, this cannot happen for every antidot, except perhaps for rather special cases requiring the antidot arrangement to be along the high-symmetry directions of the parent structure (in which the gap is expected to open up). This is in agreement with the conclusions of Ouyang et al.,[16] who showed that, in the general case, the gap can remain closed. It is also clear, on the basis of our conclusions, that the more aromatic rings are present (in the intact structure), the better it is for the aromaticity, and therefore for the gap, of the antidot structure. This is also in qualitative agreement with the conclusions of Petersen et al.,[34,35] who illustrated that a sizable gap opens when the condition $N_{Sx}/N_{Hx} > {}^1/_3$ is fulfilled, where N_{Sx} is the number of Clar sextets in the unit cell of the antidot lattice and N_{Hx} is the total number of hexagons in the unit cell. Their calculations[35] for a square lattice with lattice vectors L_x and L_y showed that the gap increases significantly only for $L_y = 3n + 1$, which is reminiscent of the condition $N = 3n + 1$ above, for the occurrence of the CIRCO (Clar) pattern. Both of these conditions (dealing with seemingly completely different but not unrelated quantities), together with the condition $N_{Sx}/N_{Hx} > {}^1/_3$, have a deeper common origin, which is the Clar CIRCO pattern. According to Clar's rules, to determine the Clar formula of a structure, there should be no more than one Clar sextet on a zigzag edge of the unit cell.[35] For pristine graphene, the Clar sextet appears every three hexagons in the direction of the zigzag and occupies one-third of the total hexagons.[17,35] Furthermore, Liu et al.[17] illustrated that these criteria are, in reality, equivalent to a more general chirality−band gap relationship that stems from the chirality-dependent atomic structures of the antidot arrangement and the Clar (i.e., CIRCO) analysis. One can therefore conclude that the various criteria in the literature[15−17,33,34] for gap opening based on aromaticity and/or chirality,[17] should in reality be related and rooted into the fundamental periodicity of the aromaticity patterns of the parent structures, expressed by the relation $N = 3n + 1$ ($n = 0, 1, 2, ...$) and the tendency to have the centers of the CIRCOs coincide with the centers of the antidots. This leads to a very intricate dependence of the size of the gap on the width and height of the parent structure ($n \times m$), as in Figures 8−10, which is, in essence, analogous to the conclusions of Petersen et al.,[34] who found that the size of the gap has a very intricate dependence on the width and height of the unit cell.

It is rather obvious, however, that our model structures, which are very small and have well-ordered antidots, are difficult or even impossible to realize experimentally, particularly for realistic applications in transistor or waveguiding devices. In addition to size, fabrication methods introduce significant levels of disorder in the shape, position, and edge configurations of individual antidots,[37] which are usually ignored in many theoretical works, including this one. Nevertheless, such model systems (similarly to many significant theoretical works based on idealized models) can still offer significant insight into much larger (more or less realistic) systems through the aromaticity conclusions and criteria that can be rather safely projected to larger sizes. The question of disorder in graphene antidot lattice devices was considered by Power and Jauho,[37] who found that antidot systems with armchair edges have a far more robust transport gap than those with zigzag or mixed edges. This is in full accord with our findings (see also ref 1) that armchair edges are significantly more aromatic than zigzag edges.

3.3. Partially Passivated Antidots. Aside from fully and totally nonpassivated antidots, in reality, it would be more common to have some sort of partial passivation, rather than the two extremes of fully passivated and totally nonpassivated antidots. In such a case, one would expect to find some intermediate behavior, which would be even more interesting scientifically because it would involve both σ and π ($\sigma + \pi$) aromaticity and/or antiaromaticity. This would be also technologically important because it would provide an additional degree of freedom for functionalization and band-gap engineering. This is indeed the case, as can be verified in Figure 12, in which three of the five vertical arrays of holes from Figure 5 (or Figure 11) are alternatively passivated, whereas the remaining two are left nonpassivated, as in Figure 12. The two nonpassivated arrays are characterized by σ-aromatic currents and the well-known CIRCO pattern with the centers of the holes weakly (but not marginally) σ-aromatic.

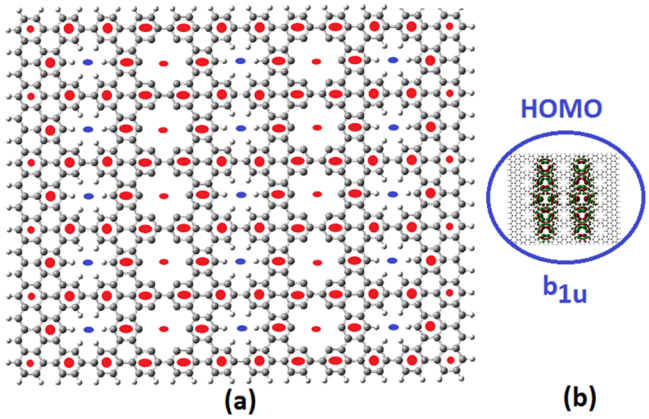

Figure 12. (a) Aromaticity pattern of the 12A × 16Z partially H-passivated (first, third, and fifth columns of holes) antidot lattice, together with (b) a micrograph of its HOMO. The second and fourth vertical arrays of holes are nonpassivated. Blue ellipses indicate antiaromaticity.

The passivated holes are characterized by π aromaticity except in the region of contact with nonpassivated holes. The

DOI: 10.1021/acs.jpcc.5b10842
J. Phys. Chem. C 2016, 120, 756−764

centers of the passivated holes are weakly (but not marginally) antiaromatic, in the sense of small positive NICS values, whereas the centers of the nonpassivated holes are weakly aromatic. As one can see, there are CIRCOs, whose centers (central rings or anti-rings) are π- or σ-aromatic or -antiaromatic and, similarly, whose peripheral rings again can be π- or σ-aromatic or -antiaromatic. This is indeed a very rich and intriguing aromaticity pattern. One could certainly have the antidots passivated in alternative ways, but the general picture should actually be similar. Obviously, one could design the desired pattern (and the resulting electronic bonding and banding properties) at will. This would have a tremendous technological and scientific significance.

4. CONCLUSIONS

It has been shown that the question of the aromaticity and the chemical bonding of antidot-decorated graphene/nanographene is complicated but very intriguing and extremely fruitful. A brief answer to the question "is antidot graphene aromatic?" (in analogy to a similar question about graphene[2]) should be yes—but not like benzene and not like graphene. The full answer strongly depends on the degree of the antidot passivation.

For totally nonpassivated antidots, the coupled aromaticity pattern of graphene gets uncoupled around the holes, revealing the primary CIRCO pattern, if geometrical and size restrictions allow it (in full agreement with our conclusions in ref 1). In such a case, the following comments apply:

- The design of the antidot lattice (pre)selects from all possible aromaticity patterns the one in which the centers of the holes coincide with the centers of the CIRCO subunits, in an attempt to maximize the number of aromatic rings on the rims. This is very important for functionalization.
- Moreover, in contrast to graphene, the decoupled primary CIRCO aromaticity pattern of the periodic antidot arrangement can be totally or partially σ-aromatic. This is corroborated by the structure of the frontier orbitals around the Fermi level, which, in contrast to that in pure graphene, is dominated by σ orbitals.
- The centers of the holes, which also comprise the centers of the corresponding CIRCOs, are weakly σ-aromatic (NICS of about −6 ppm) or even nonaromatic.
- The σ-aromatic CIRCOs are fully compatible with Clar's rules, although Clar's rules have been invoked for π aromaticity. This reveals the importance of σ bonding in the structural properties of graphene (or even benzene) and (strangely, as it might appear) supports the idea[30] that Clar's sextet rule could be a consequence of the σ-electron framework.
- Thus, the aromaticity pattern of the nonpassivated antidot lattice consists of the primary CIRCO Clar-type aromaticity pattern of graphene in which the aromaticity is of σ type (cf. Figure 6b).

For fully passivated antidots, the decoupling of the aromaticity pattern primarily involves the finite surfaces (edges) of the intact nanographene, and secondarily the centers of the antidots. Thus, in the majority of the cases, the aromaticity pattern of the fully passivated antidots coincides with the aromaticity pattern of the parent structure, except for the region of the holes. Threfore, the aromaticity of the fully passivated antidot nanographenes follows the periodicities and regularities of the parent nanographene structures,[1] which are inherently linked to chirality.[17] Furthermore, in this case, one can make the following statements:

- The aromaticity is of the common π type.
- The centers of the holes (or else, the empty rings) are weakly σ-antiaromatic (NICS value of about +6 ppm) or even nonaromatic
- Thus, the aromaticity pattern of the fully passivated antidot lattice should be similar to the primary aromaticity pattern of graphene in which the centers of the antidots (and of the corresponding CIRCO centers) would be weakly σ-antiaromatic (like Figure 11b).

For partially passivated antidots the situation is almost intermediate, as in Figure 12a. As the degree of passivation increases, the σ aromaticity gradually fades away, and in the limit of full passivation, finally the aromaticity pattern becomes increasingly "insensitive" to details approaching the corresponding π-arromaticity pattern of the intact graphene system. Thus, one can state the following:

- The type and extent of antidot passivation could be an additional degree of freedom for the band-gap engineering of graphene antidots.
- The present results should be extremely important, not only for future technological applications but also for a fundamental scientific understanding of aromaticity.

AUTHOR INFORMATION

Corresponding Author

*E-mail: Zdetsis@upatras.gr.

Notes

The authors declare no competing financial interest.

ACKNOWLEDGMENTS

This work was supported by EU-ERC Project PHOTOMETA No. 320081

REFERENCES

(1) Zdetsis, A. D.; Economou, E. N. A Pedestrian Approach to the Aromaticity of Graphene and Nanographene: Significance of Huckel's $(4n + 2)\pi$ Electron Rule. *J. Phys. Chem. C* **2015**, *119*, 16991−17003.
(2) Popov, I. A.; Bozhenko, K. V.; Boldyrev, A. I. Is Graphene Aromatic? *Nano Res.* **2012**, *5*, 117−123.
(3) Moran, D.; Stahl, F.; Bettinger, H. F.; Schaefer, H. F., III; Schleyer, P. v. R. Towards Graphite: Magnetic Properties of Large Polybenzenoid Hydrocarbons. *J. Am. Chem. Soc.* **2003**, *125*, 6746−6752.
(4) Schleyer, P. v. R. Introduction: Aromaticity. *Chem. Rev.* **2001**, *101*, 1115−1118.
(5) Schleyer, P.v.R. Introduction: Delocalization−Pi and Sigma. *Chem. Rev.* **2005**, *105*, 3433−3435.
(6) Novoselov, K. S.; Jiang, D.; Schedin, F.; Booth, T. J.; Khotkevich, V. V.; Morozov, S. V.; Geim, A. K. Two-Dimensional Atomic Crystals. *Proc. Natl. Acad. Sci. U. S. A.* **2005**, *102*, 10451−10453.
(7) Geim, A. K.; Novoselov, K. S. The Rise of Graphene. *Nat. Mater.* **2007**, *6*, 183−191.
(8) Pauling, L. *The Nature of the Chemical Bond and the Structure of Molecules and Crystals: An Introduction to Modern Structural Chemistry*; Cornell University Press: Ithaca, NY, 1960.
(9) Zubarev, D. Y.; Frenklach, M.; Lester, W. A., Jr. From Aromaticity to Self-organized Criticality in Graphene. *Phys. Chem. Chem. Phys.* **2012**, *14*, 12075−12078.
(10) Martin-Martinez, F. J.; Fias, S.; Van Lier, G.; De Proft, F.; Geerlings, P. Tuning Aromaticity Patterns and Electronic Properties of

DOI: 10.1021/acs.jpcc.5b10842
J. Phys. Chem. C 2016, 120, 756−764

Armchair Graphene Nanoribbons with Chemical Edge Functionalisation. *Phys. Chem. Chem. Phys.* **2013**, *15*, 12637−12647.
(11) Martin-Martinez, F. J.; Fias, S.; Hajgato, B.; Van Lier, G.; De Proft, F.; Geerlings, P. Inducing Aromaticity Patterns and Tuning the Electronic Transport of Zigzag Graphene Nanoribbons via Edge Design. *J. Phys. Chem. C* **2013**, *117*, 26371−26384.
(12) Matsuo, Y.; Tahara, K.; Nakamura, E. Theoretical Studies on Structures and Aromaticity of Finite-Length Armchair Carbon Nanotubes. *Org. Lett.* **2003**, *5*, 3181−3184.
(13) Pedersen, T. G.; Flindt, C.; Pedersen, J.; Jauho, A. P.; Mortensen, N. A.; Pedersen, K. Optical Properties of Graphene Antidot Lattices. *Phys. Rev. B: Condens. Matter Mater. Phys.* **2008**, *77*, 245431.
(14) Pedersen, T. G.; Flindt, C.; Pedersen, J.; Mortensen, N. A.; Jauho, A. P.; Pedersen, K. Graphene Antidot Lattices: Designed Defects and Spin Qubits. *Phys. Rev. Lett.* **2008**, *100*, 136804.
(15) Kim, M.; Safron, N. S.; Han, E.; Arnold, M. S.; Gopalan, P. Fabrication and Characterization of Large-Area, Semiconducting Nanoperforated Graphene Materials. *Nano Lett.* **2010**, *10*, 1125−1131.
(16) Ouyang, F.; Peng, S.; Liu, Z.; Liu, Z. Bandgap Opening in Graphene Antidot Lattices: The Missing Half. *ACS Nano* **2011**, *5*, 4023−4030.
(17) Liu, X.; Zhang, Z.; Guo, W. Universal Rule on Chirality-Dependent Bandgaps in Graphene Antidot Lattices. *Small* **2013**, *9*, 1405−1410.
(18) Fürst, J. A.; Pedersen, J. G.; Flindt, C.; Mortensen, N. A.; Brandbyge, M.; Pedersen, T. G.; Jauho, A.-P. Electronic Properties of Graphene Antidot Lattices. *New J. Phys.* **2009**, *11*, 095020.
(19) Ebbesen, T. W.; Lezec, H. J.; Ghaemi, H. F.; Thio, T.; Wolff, P. A. Extraordinary Optical Transmission through Sub-Wavelength Hole Arrays. *Nature* **1998**, *391*, 667−669.
(20) Pendry, J. B.; Schurig, D.; Smith, D. R. Controlling Electromagnetic Fields. *Science* **2006**, *312*, 1780−1782.
(21) Tassin, P.; Koschny, Th.; Soukoulis, C. M. Graphene for Terahertz Applications. *Science* **2013**, *341*, 620−621.
(22) Basharin, A. A.; Mavidis, C.; Kafesaki, M.; Economou, E. N.; Soukoulis, C. M. Epsilon Near Zero Based Phenomena in Metamaterials. *Phys. Rev. B: Condens. Matter Mater. Phys.* **2013**, *87*, 155130.
(23) Schleyer, P.v.R.; Maerker, C.; Dransfeld, A.; Jiao, H.; van Eikema Hommes, N. J. R. Nucleus Independent Chemical Shifts: A Simple and Efficient Aromaticity Probe. *J. Am. Chem. Soc.* **1996**, *118*, 6317−6318.
(24) Sola, M.; Feixas, F.; Jimenez-Halla, J. O.C.; Matito, E.; Poater, J. A Critical Assessment of the Performance of Magnetic and Electronic Indices of Aromaticity. *Symmetry* **2010**, *2*, 1156−1179.
(25) Tsipis, A. C.; Depastas, I. G.; Tsipis, C. A. Diagnosis of the σ-, π- and ($\sigma + \pi$)-Aromaticity by the Shape of the NICSzz-Scan Curves and Symmetry-Based Selection Rules. *Symmetry* **2010**, *2*, 284−319.
(26) Tsipis, C. A. Aromaticity/Antiaromaticity in "Bare"and "Ligand-Stabilized" Rings of Metal Atoms. *Struct. Bonding (Berlin, Ger.)* **2010**, *136*, 217−274.
(27) Frisch, M. J.; Trucks, G. W.; Schlegel, H. B.; Scuseria, G. E.; Robb, M. A.; Cheeseman, J. R.; Scalmani, G.; Barone, V.; Mennucci, B.; Petersson, G. A.; Nakatsuji, H.; Caricato, M.; Li, X.; Hratchian, H. P.; Izmaylov, A. F.; Bloino, J.; Zheng, G.; Sonnenberg, J. L.; Hada, M.; Ehara, M.; Toyota, K.; Fukuda, R.; Hasegawa, J.; Ishida, M.; Nakajima, T.; Honda, Y.; Kitao, O.; Nakai, H.; Vreven, T.; Montgomery, J. A., Jr.; Peralta, J. E.; Ogliaro, F.; Bearpark, M.; Heyd, J. J.; Brothers, E.; Kudin, K. N.; Staroverov, V. N.; Keith, T.; Kobayashi, R.; Normand, J.; Raghavachari, K.; Rendell, A.; Burant, J. C.; Iyengar, S. S.; Tomasi, J.; Cossi, M.; Rega, N.; Millam, J. M.; Klene, M.; Knox, J. E.; Cross, J. B.; Bakken, V.; Adamo, C.; Jaramillo, J.; Gomperts, R.; Stratmann, R. E.; Yazyev, O.; Austin, A. J.; Cammi, R.; Pomelli, C.; Ochterski, J. W.; Martin, R. L.; Morokuma, K.; Zakrzewski, V. G.; Voth, G. A.; Salvador, P.; Dannenberg, J. J.; Dapprich, S.; Daniels, A. D.; Farkas, Ö.; Foresman, J. B.; Ortiz, J. V.; Cioslowski, J.; Fox, D. J. *Gaussian 09*, revision C.01; Gaussian, Inc.: Wallingford, CT, 2009.
(28) Adamo, C.; Barone, V. Toward Reliable Density Functional Methods Without Adjustable Parameters: The PBE0 Model. *J. Chem. Phys.* **1999**, *110*, 6158−6169.
(29) Zdetsis, A. D. Structural, Cohesive, Electronic, and Aromatic Properties of Selected Fully and Partially Hydrogenated Carbon Fullerenes. *J. Phys. Chem. C* **2011**, *115*, 14507−14516.
(30) Maksić, Z. B.; Barić, D.; Müller, T. Clar's Sextet Rule Is a Consequence of the σ-Electron Framework. *J. Phys. Chem. A* **2006**, *110*, 10135−10147.
(31) Popov, A.; Boldyrev, A. I. Deciphering Chemical Bonding in a BC_3 Honeycomb Epitaxial Sheet. *J. Phys. Chem. C* **2012**, *116*, 3147−3152.
(32) Popov, A.; Li, Y.; Chen, Z.; Boldyrev, A. I. "Benzation" of Graphene upon Addition of Monovalent Chemical Species. *Phys. Chem. Chem. Phys.* **2013**, *15*, 6842−6848.
(33) Petersen, R.; Pedersen, T. G.; Jauho, A. P. Clar Sextet Analysis of Triangular, Rectangular, and Honeycomb Graphene Antidot Lattices. *ACS Nano* **2011**, *5*, 523−529.
(34) Petersen, R.; Pedersen, T. G.; Jauho, A. P. Clar Sextets in Square Graphene Antidot Lattices. *Phys. E* **2012**, *44*, 967−970.
(35) Ouyang, F.; Yang, Z.; Peng, S.; Zheng, X.; Xiong, X. Antidot-Dependent Bandgap and Clar Sextets in Graphene Antidot Lattices. *Phys. E* **2014**, *56*, 222−226.
(36) Zdetsis, A. D.; Sigalas, M. M.; Koukaras, E. N. Ab Initio Theoretical Investigation of Beryllium and Beryllium Hydride Nanoparticles and Nanocrystals with Implications for the Corresponding Infinite Systems. *Phys. Chem. Chem. Phys.* **2014**, *16*, 14172−14182.
(37) Power, S. R.; Jauho, A.-P. Electronic Transport in Disordered Graphene Antidot Lattice Devices. *Phys. Rev. B: Condens. Matter Mater. Phys.* **2014**, *90*, 115408.

DOI: 10.1021/acs.jpcc.5b10842
J. Phys. Chem. C 2016, 120, 756−764